JACS Au
AN OPEN ACCESS JOURNAL OF THE AMERICAN CHEMICAL SOCIETY

pubs.acs.org/jacsau
Article

Simultaneous Live Mapping of pH and Hydrogen Peroxide Fluctuations in Autophagic Vesicles

Smitaroopa Kahali, Ranojoy Baisya, Sayani Das, and Ankona Datta*

Cite This: JACS Au 2025, 5, 343−352
Read Online

ACCESS | Metrics & More | Article Recommendations | Supporting Information

ABSTRACT: Hydrogen peroxide (H_2O_2) plays a critical role in the regulation and progress of autophagy, an essential recycling process that influences cellular homeostasis and stress response. Autophagy is characterized by the formation of intracellular vesicles analogous to recycle "bags" called autophagosomes, which fuse with lysosomes to form autolysosomes, eventually ending up as lysosomes. We have developed two novel autophagic vesicle-targeted peptide-based sensors, **ROSA** for H_2O_2 and **pHA** for pH, to simultaneously track H_2O_2 and pH dynamics within autophagic vesicles as autophagy advances. Since pH values progressively decrease within autophagic vesicles with the progress of autophagy, we utilized information on vesicular pH to identify stages of autophagic vesicles in live cells. Fluorescence intensities of the H_2O_2 sensor, **ROSA**, within autophagic compartments at different autophagic stages, which were identified by simultaneous pH mapping, revealed that H_2O_2 levels vary significantly within autophagic vesicles as autophagy progresses, with maximum H_2O_2 levels in the autolysosomal stage. This study provides the first detailed observation of H_2O_2 fluctuations within autophagic vesicles throughout the entire process of autophagy in living mammalian cells, offering insights into the oxidative changes associated with this vital cellular process.

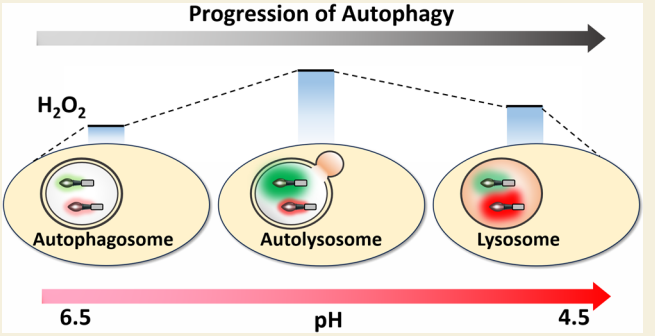

KEYWORDS: *autophagy, H_2O_2 sensor, pH sensor, autophagic vesicle-targeted H_2O_2 sensor, autophagic vesicle-targeted pH sensor, simultaneous detection of bioanalytes, simultaneous pH and H_2O_2 detection in autophagic vesicles, tracking H_2O_2 in autophagy, autophagic vesicle-targeted fluorescent sensor, H_2O_2 fluctuations in autophagy*

Autophagy is an essential biological process which enables cells to recycle damaged and dysfunctional components and plays a central role in immunity, tumor suppression, and slowing down aging.[1−5] Dysregulation of autophagy is associated with various pathophysiological conditions including neurodegeneration, metabolic disorders like diabetes, cardiovascular diseases, autoimmune diseases, and cancer.[1,3−5] While there are several mechanisms underlying autophagy, macroautophagy, in which an isolation membrane forms within a cell and encloses substances to be degraded, is the most ubiquitous.[1] The vesicle formed as a result is called an autophagosome. Autophagosomes fuse with lysosomes in later stages of autophagy to form autolysosomes, which finally end up as lysosomes. Hence, autophagy is akin to a recycling factory in which unused proteins and organelles are degraded and starting materials for resynthesis of macromolecules are released back into the cell. Autophagy is tightly regulated. Along with several protein players, small molecules and ions are critical regulators and markers of the progress of autophagy or the autophagic flux. Importantly, stagewise information on levels of analytes within autophagic vesicles can provide a way to map the process and alterations during pathophysiological conditions, thereby allowing the screening of autophagy modulators as drugs. However, there have been barely any attempts toward simultaneous monitoring of endogenous bioanalytes within autophagic compartments. In this context, we sought to track the correlated dynamics of pH and H_2O_2 with the progress of autophagy in living cells.

Why this combination of analytes? Proton concentration increases and hence pH decreases progressively from 6.5 to 4.5, as autophagy advances.[6] Mapping pH within autophagic compartments can therefore be used to identify the stage of an autophagic vesicle.[6,7] Tracking a second analyte along with pH will provide information on how the levels of the analyte vary as autophagy progresses. The second analyte that we selected to detect was H_2O_2. Among the several factors that can influence the initiation and progress of autophagy, reactive oxygen species (ROS) is one of the most significant.[8−13] Reports suggest that ROS, particularly H_2O_2, participates in the regulation of autophagy.[9,10,13] H_2O_2 at physiological levels

Received: October 29, 2024
Revised: December 21, 2024
Accepted: January 2, 2025
Published: January 15, 2025

can trigger autophagy as a protective response. This aids cells to adapt to stressors promoting survival and longevity.[10,11] However, excess H_2O_2 can lead to autophagic failure, which in turn can result in cell death.[10,11,13] Dysregulation of H_2O_2-mediated signaling and autophagy has been associated with the pathogenesis of several disorders.[13−27] Neurodegenerative diseases like Alzheimer's and Parkinson's diseases involve impaired autophagic clearance of misfolded proteins and damaged organelles, exacerbated by oxidative stress.[15−18] Excessive increase in H_2O_2 and inhibition of autophagy also occur during cardiac ischemia.[20−22] Cancer cells can exploit altered H_2O_2 levels and autophagy to promote survival and resistance to therapy.[19,25,28] Misregulated autophagy and oxidative stress are also linked to aging and metabolic disorders like diabetes and obesity.[23,24,26,27] The intricate interplay between autophagy and H_2O_2 necessitates tracking H_2O_2 across different autophagic stages, which can be achieved via the simultaneous tracking of pH and H_2O_2 within autophagic compartments.

Thus far, either overall cellular H_2O_2 levels or lysosomal H_2O_2 under different autophagy triggering conditions have been studied.[29−37] However, there is no stagewise information on H_2O_2 levels within autophagic vesicles during the progress of autophagy in live cells. Therefore, many questions remain unanswered. These include: At which stage of autophagy is the level of H_2O_2 maximum within autophagic vesicles? How do the levels of H_2O_2 inside autophagic vesicles change in response to different stressors? How do the levels of H_2O_2 within autophagic compartments influence the initiation and progress of autophagy? How are the levels of autophagosomal H_2O_2 related to the pathogenesis of different diseases? Answering these questions will open avenues for exploring therapeutic ideas aimed at treating autophagy and H_2O_2-mediated pathophysiological conditions; however, the key lies in the ability to obtain information on the intrinsic/endogenous levels of H_2O_2 within autophagic compartments at different stages of autophagy.

Sensing H_2O_2 inside autophagic vesicles at different stages of autophagy is nontrivial because of the following factors. Autophagosomes are transient double-membrane structures that engulf cellular cargo and undergo fusion with lysosomes to form autolysosomes where cargo degradation starts.[38] Hence, detecting H_2O_2 within autophagosomes during their formation, maturation, and fusion stages would require a technique with a high spatiotemporal resolution. Fluorescence confocal microscopy can provide the apt resolution across space and time. But H_2O_2 levels are tightly regulated within cellular compartments and fluctuate rapidly in response to cellular stress or signaling events. In order to monitor these transient fluctuations within autophagic vesicles, an autophagosome-targeted, rapid-response fluorescent sensor is required, which will quickly and accurately detect changes in endogenous H_2O_2 levels. Simultaneous live-imaging with an orthogonally emitting autophagosome-targeted pH-responsive fluorescent sensor will provide complete information on how the levels of H_2O_2 change within autophagic compartments as autophagy advances.

To achieve this goal, we have developed two novel sensors: 1. a cell-permeable, autophagic vesicle-targeted, small-molecule peptide conjugate-based fluorescent sensor (**ROSA**) for detecting H_2O_2 and 2. an orthogonally emitting cell-permeable, autophagic vesicle-targeted, pH-sensitive, small-molecule peptide conjugate-based fluorescent sensor (**pHA**) used for simultaneously tracking the autophagic flux (Figure 1). Additionally, we have also utilized a previously reported ratiometric autophagosome-targeted pH sensor from our group (**HCFP**)[7] to identify the stages of autophagic vesicles, i.e., to distinguish between autophagosomes, autolysosomes, and lysosomes. Using different combinations of **ROSA** with either **pHA** or **HCFP**, we show for the first time that the levels of H_2O_2 increase within autophagic vesicles with the progress of autophagy and peak at the autolysosomal stage.

RESULTS AND DISCUSSION

ROSA and **pHA** were designed to include a targeting peptide sequence and either an H_2O_2- or a pH-sensitive dye,

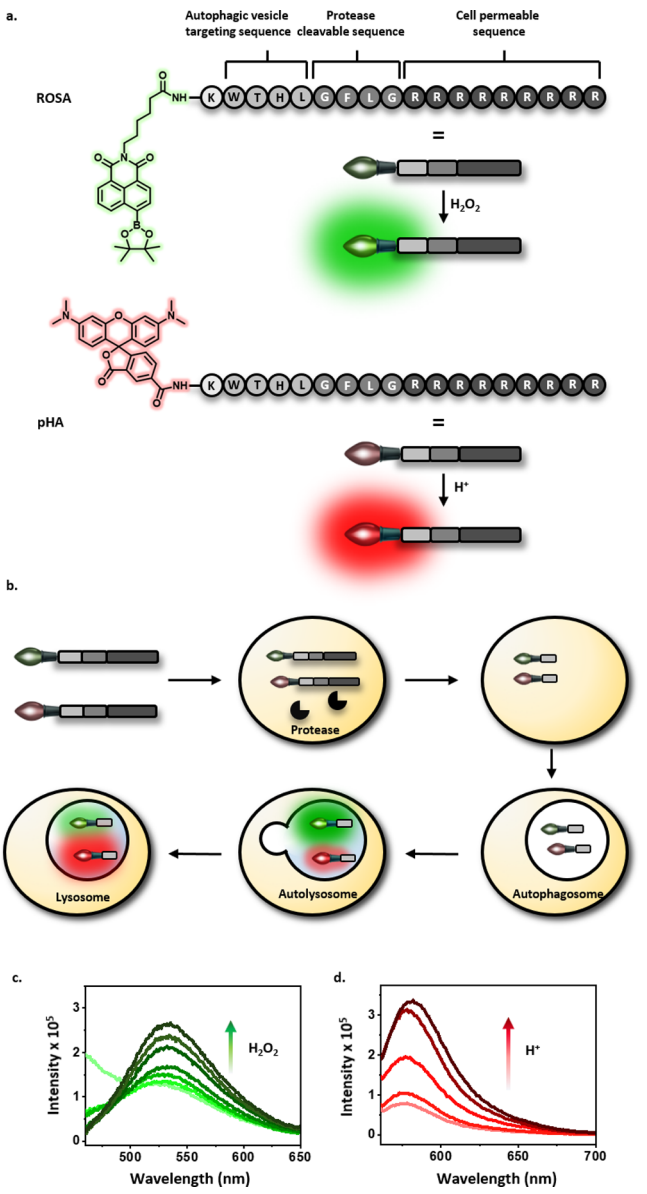

Figure 1. (a) Design of novel sensors, **ROSA** and **pHA**, for detecting H_2O_2 levels and pH, respectively, inside autophagic vesicles during the progress of autophagy. (b) Scheme depicting tracking of H_2O_2 and pH fluctuations by **ROSA** and **pHA** during different stages of autophagy. (c) Fluorescence response of **ROSA** (10 μM) to H_2O_2 (0−560 μM) in HEPES (20 mM) buffer (pH 7.4); λ_{ex} 378 nm. (d) Fluorescence response of **pHA** (10 μM) to pH (3 to 8) in the HEPES (20 mM) buffer; λ_{ex} 540 nm.

https://doi.org/10.1021/jacsau.4c01021
JACS Au 2025, 5, 343−352

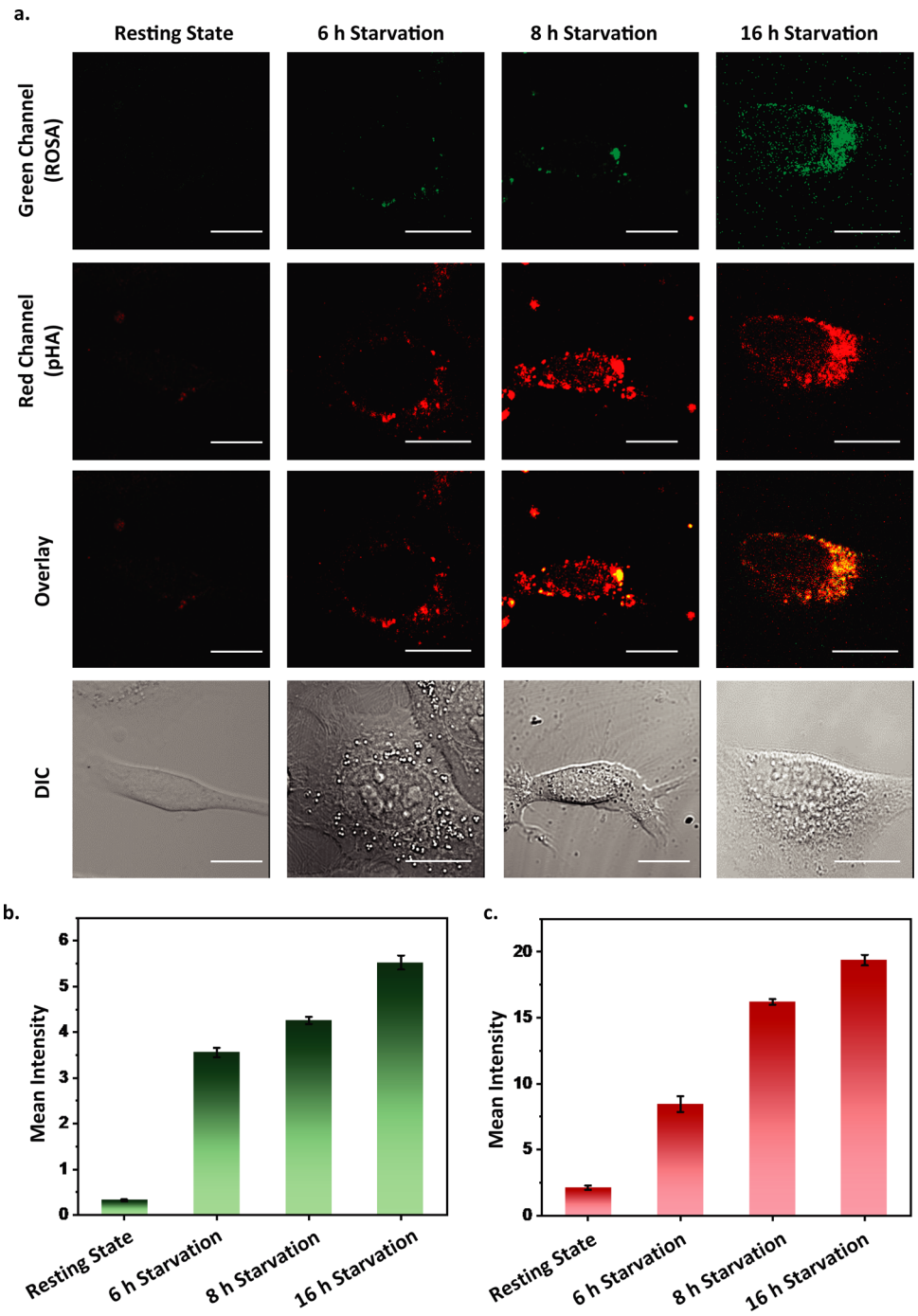

Figure 2. (a) Representative confocal single z plane images of HeLa cells (first panel: green channel **ROSA**; λ_{ex} = 405 nm, λ_{em} = 500−545 nm; second panel: red channel **pHA**; λ_{ex} = 543 nm, λ_{em} = 575−650 nm; third panel: overlay between green and red channels; fourth panel: differential contrast images). Scale bar: 10 μm. Different sets of HeLa cells were starved for 0 (resting state), 6, 8, and 16 h, respectively, then incubated with **ROSA** (10 μM) in aqueous media for 30 min, washed and incubated with **pHA** (10 μM) in aqueous media for 30 min, and washed and imaged. Bar plots representing mean intensities obtained from intensity analysis of four sets of cell imaging experiments using **ROSA** (b) and **pHA** (c); representative images shown in panel (a). Data are presented as SEM, where n = 6 in each set.

respectively (Figure 1). The role of the peptide was to impart cell permeability to the construct and targetability to autophagic vesicles. The targeting peptide sequence was based on an earlier successful design of an autophagic vesicle-targeting sequence from our group.[7] For the sake of completeness, we also describe the design here. Briefly, the sequence consisted of an LC3 protein-binding segment, a Cathepsin B cleavable site, and a polyarginine unit. LC3 is a member of the Atg8 protein family, known for its localization on autophagic vesicles.[39] Autophagic receptor proteins, such as p62, possess Atg8 interaction motifs responsible for cargo recognition. These interaction motifs have a typical peptide sequence **W-X-X-L**, in which a tryptophan and a leucine are separated by two amino acids.[39−41] In this context, the peptide sequence **W-T-H-L** has been widely reported to target autophagic vesicles.[39−41] A nonamer of arginine ($\mathbf{R_9}$) was added to the sequence to make the probe cell-permeable. Since polyarginine sequences tend to target either the nucleus or

https://doi.org/10.1021/jacsau.4c01021
JACS Au 2025, 5, 343−352

endosomes,[42] a Cathepsin B cleavable site **G-F-L-G** was placed between **W-T-H-L** and $\mathbf{R_9}$. Therefore, the final sequence for both **ROSA** and **pHA** was **W-T-H-L-G-F-L-G-R$_9$**. Next, we selected the sensing units.

1,8-Napthalimide with a boronic ester cap has been widely used as an activity-based probe for detecting H_2O_2.[43−46] H_2O_2 removes the boronic ester cap and converts it to a hydroxyl group, thus generating an electron donor−acceptor configuration, leading to an enhancement in the fluorescence response.[43−46] This family of dyes has been proven to be selective toward H_2O_2 over other ROS species.[41] Hence, the construct mentioned above was used as the H_2O_2-selective and sensitive moiety. The design of the dye also consisted of a hexanoic acid linked to the imide position for attachment to the peptide unit. As the pH-sensitive dye, 5(6)-carboxytetramethylrhodamine was used, owing to the pH-sensitive behavior of rhodamine-based dyes.[47] Both dyes were first attached to lysine. Following that, the lysine−dye conjugates were attached to the autophagic vesicle-targeting peptide sequence to afford the novel sensors **ROSA** and **pHA** (Schemes S1 and S2). Both sensors were characterized via liquid chromatography/electrospray ionization mass spectrometry (LC/ESI-MS) (Figures S1 and S2).

ROSA and **pHA** were completely water−soluble in the tested concentrations of up to 2 mM. Therefore, all experiments were carried out in an aqueous buffer. The fluorescence response of **ROSA** in the presence of increasing concentrations of H_2O_2 was recorded (Figures 1c and S3). Upon excitation at 378 nm, **ROSA** exhibited a peak with the maxima at 530 nm, which underwent a 2-fold enhancement in the presence of H_2O_2 (Figures 1c and S3). The fluorescence response of **ROSA** was also checked in the presence of other biologically relevant analytes like Cl^-, NO_3^-, HCO_3^-, glutathione, and ascorbic acid (Figure S4). No change in fluorescence was observed with any of the previously mentioned analytes (Figure S4). Since **ROSA** was designed to target the autophagic vesicles and the pH of the autophagic vesicles changed from 6−6.5 to 4.5 during the progression of autophagy, we investigated the response of **ROSA** at pH 4.5 in order to eliminate the possibility of interference from changing pH. No change in fluorescence was observed (Figure S4) and an identical response to H_2O_2 was retained at lower pH (Figure S5). This result indicated that the response of **ROSA** toward H_2O_2 was indeed unaffected by pH.

Next, the pH-dependent fluorescence response of **pHA** was recorded (Figures 1d and S6). Upon excitation at 540 nm, **pHA** exhibited a peak with the maxima at 582 nm, which increased 4.5 times in intensity with decreasing pH from 8 to 3 (Figures 1d and S6). Furthermore, the response of **pHA** was checked in the presence of biologically relevant metal ions (Na^+, K^+, Mg^{2+}, Ca^{2+}, Mn^{2+}, Fe^{2+}) and glutathione at their physiologically relevant concentrations. No significant increase in emission was observed for any of these analytes (Figure S7), thus establishing the selectivity of **pHA** toward pH changes. As a control, the response of **pHA** was also checked in the presence of H_2O_2. No change in fluorescence was observed, and the pH-dependent response was retained in the presence of H_2O_2 (Figure S8). Therefore, **ROSA** and **pHA** were orthogonally emitting probes with no cross-talk between the respective analytes to which each probe responded to.

Hence, we tested the applicability of **ROSA** and **pHA** for the simultaneous tracking of pH and H_2O_2 within autophagic compartments with the progression of autophagy in living cells. Both the sensors permeated living cells within 30 min of direct incubation. Very low fluorescence was observed in both green (**ROSA**; λ_{ex} = 405 nm) and red (**pHA**; λ_{ex} = 543 nm) channels when healthy HeLa cells at the resting state were incubated with the two sensors (Figure 2a, first column). This is in accordance with the fact that cells at the resting state have a low number of autophagic vesicles.[48] When HeLa cells were starved for 8 h or more, an increase in punctate-like fluorescence was observed in both channels, indicating an increased autophagic flux (Figures 2a, S9 and S10). The percentage of labeled cells was further calculated from fluorescence confocal images of both the sensors taken with a wide field of view. In cells starved for 8−16 h in multiple cell plates (N = 5, n = 14−50), the percentage of cells labeled by **ROSA** was 94.3 ± 1.8% and that by **pHA** was 100% (Figure S11). To ensure that there was no bleed-through between **pHA** and **ROSA** emission channels, cells were only incubated with **ROSA** and imaged at the excitation wavelength and emission channel of **pHA** and vice versa (Figure S12). In both cases, negligible fluorescence was observed from the other channel, confirming that there was no cross-talk between the responses of the two probes in live cell imaging (Figure S12). Simultaneous imaging with **ROSA** and **pHA** in starved cells indicated a significant colocalization between the two channels, thus ensuring that both **ROSA** and **pHA** reached the same intracellular region (Figure S13).

To confirm that the generated punctate structures were indeed autophagic vesicles, colocalization studies of **ROSA** and **pHA** were performed with cyan fluorescent protein-tagged LC3 (CFP-LC3) and green fluorescent protein-tagged LC3 (GFP-LC3), respectively (Figure S14). As controls, starved cells were also incubated with only **ROSA** or only **pHA** and imaged at the excitation wavelengths and emission channels of CFP-LC3 and GFP-LC3, respectively (Figure S15). Further, CFP-LC3-transfected cells were imaged at the emission channel of **ROSA**- and GFP-LC3-transfected cells were imaged at the excitation wavelength and emission channel corresponding to **pHA** (Figure S15). In all four cases, negligible fluorescence was observed, thus negating the possibility of bleed-through (Figure S15). When imaged together, **ROSA** afforded a clear colocalization with CFP-LC3 (Mander's coefficients: M1 = 0.59 and M2 = 0.67) (Figure S14a). A significant colocalization was also observed between **pHA** and GFP-LC3 (Mander's coefficients: M1 = 0.65, M2 = 0.64) (Figure S14b). These results showed that both **ROSA** and **pHA** could successfully target autophagic vesicles.

Encouraged by the results, we ventured to understand the effect of prolonged starvation on autophagy and H_2O_2 levels in autophagic vesicles. Hence, HeLa cells were starved for 0, 6, 8, and 16 h, respectively, since significant levels of autophagic vesicles have been reported to be generated in cells upon prolonged starvation starting from 6 h.[13,49,50] A gradual increase in punctate-like fluorescence was observed in both channels with increasing starvation time (Figure 2). Starvation initiates the progression of autophagy[49,50] and during the process, the pH inside the autophagic vesicles changes from 6−6.5 to 4.5. Since **pHA** turns on at lower pH, the observed increase in the fluorescence of **pHA** with increasing starvation time indicated an increase in the autophagic flux. Furthermore, along with the increase in the autophagic flux, the enhancement in the fluorescence intensity of **ROSA** that we observed, indicated a surge in the endogenous H_2O_2 levels within autophagic compartments.

https://doi.org/10.1021/jacsau.4c01021
JACS Au 2025, 5, 343−352

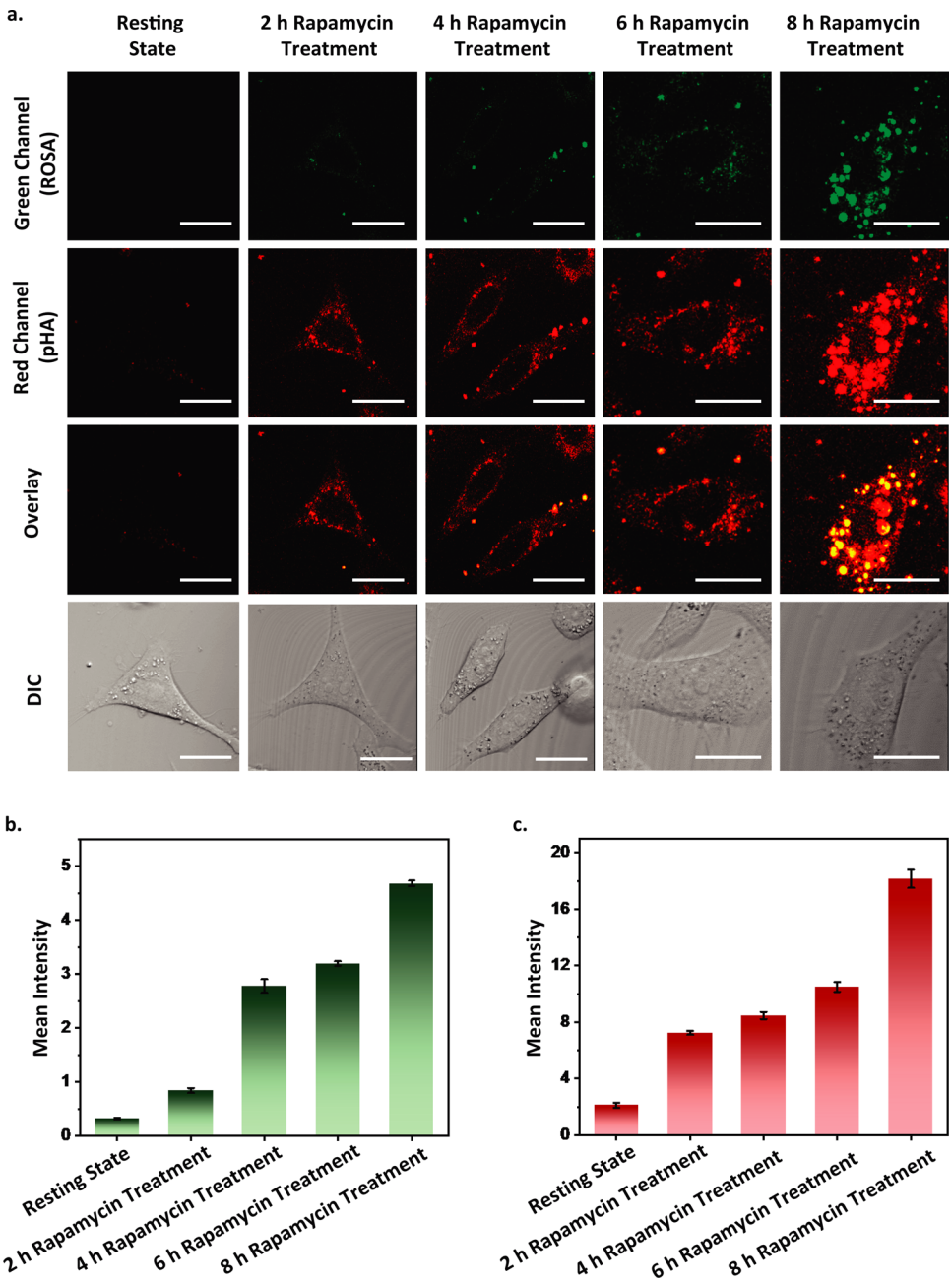

Figure 3. (a) Representative confocal single z plane images of HeLa cells (first panel: green channel, **ROSA**; λ_{ex} = 405 nm, λ_{em} = 500−545 nm; second panel: red channel, **pHA**; λ_{ex} = 543 nm, λ_{em} = 575−650 nm; third panel: overlay between green and red channels; fourth panel: differential contrast images). Scale bar: 10 μm. Different sets of HeLa cells were incubated with Rapamycin (100 nM) for 0 (resting state), 2, 4, 6, and 8 h respectively, then incubated with **ROSA** (10 μM) in aqueous media for 30 min, washed and incubated with **pHA** (10 μM) in aqueous media for 30 min, and washed and imaged. Bar plots representing mean intensities obtained from intensity analysis of four sets of cell imaging experiments using **ROSA** (b) and **pHA** (c); representative images shown in panel (a). Data are presented as SEM where n = 6 in each set.

Next, we explored the effect of a known autophagy trigger, Rapamycin. Rapamycin inhibits the Ser/Thr protein kinase mammalian target of Rapamycin (mTOR), disrupting signals crucial for cell growth and proliferation, thereby promoting cellular starvation and increasing autophagy. Living HeLa cells were incubated with Rapamycin for 0, 2, 4, 6, and 8 h respectively, then with **ROSA** and **pHA**, and imaged (Figure 3a). A gradual increase in the red channel (**pHA**) within punctate structures was observed with increasing incubation times of Rapamycin, which indicated an increase in the autophagic flux (Figure 3a). However, an increase in the fluorescence of **ROSA** within the puncta was only observed after 4 h of Rapamycin treatment and a significant increase was observed after 8 h of Rapamycin treatment (Figure 3a). This result revealed that although there was an increase in the autophagic flux already at 2 h of Rapamycin treatment, H_2O_2 levels only increased after 4 h of Rapamycin treatment and underwent a substantial increase after 8 h of Rapamycin treatment (Figure 3b). We also noted that during cell starvation, the rise in H_2O_2 levels within autophagic vesicles occurred gradually, whereas with Rapamycin treatment, the increase in H_2O_2 levels was abrupt. Therefore, we concluded that fluctuations in H_2O_2 concentrations inside autophagic vesicles as autophagy progresses vary with the trigger.

https://doi.org/10.1021/jacsau.4c01021
JACS Au 2025, 5, 343−352

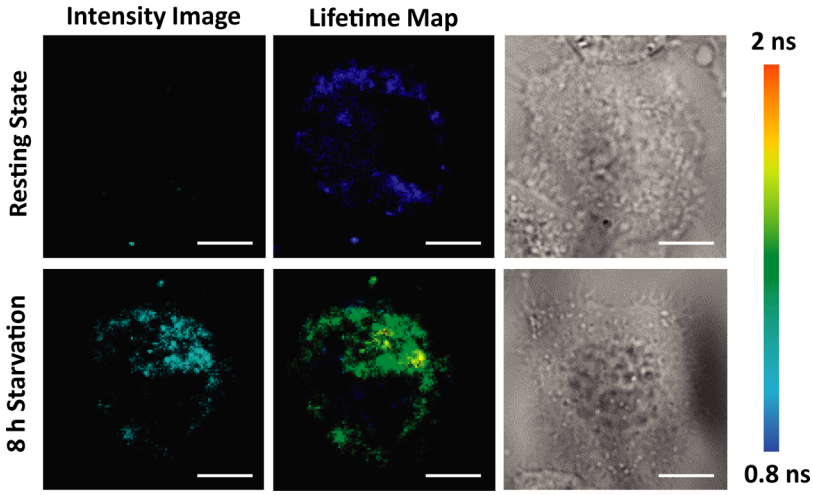

Figure 4. Representative confocal single *z* plane intensity images (left) and lifetime maps (right) of HeLa cells. Cells were incubated with **ROSA** (10 μM) for 30 min, washed, and imaged (top panel). Cells were starved for 8 h, incubated with **ROSA** (10 μM) for 30 min, washed, and imaged (bottom panel). Scale bar: 10 μm.

At the resting state, the fluorescence intensity of **ROSA** inside cells is almost negligible. To ensure that **ROSA** entered autophagic vesicles at the autophagosome stage and not at a later stage which would convolute the interpretation of the imaging data, we conducted fluorescence lifetime imaging (FLIM) of **ROSA** in cells at both resting and starved conditions (Figures 4 and S16). At the resting state, we observed punctate-like regions with a lower lifetime (0.8 ns) in all of the cells within the plate imaged (Figures 4 and S16). The fluorescence lifetime of 1,8-napthalimide with a boronic ester cap is reported.[51] The in-cell lifetime values obtained from punctate-like regions in cells at the resting state matched with the reported value of 1 ns.[51] Therefore, **ROSA** reached autophagic vesicles at early stages but the fluorescence was low owing to the nonsignificant levels of H_2O_2 in early autophagosomes, distinctly validating the conclusions that we drew from the intensity images (Figures 2 and 3).

When the same experiment was conducted on starved cells, the fluorescence lifetime inside the punctate regions increased (1.6 ns) (Figures 4 and S16b), as expected.[51] This result convincingly demonstrated that the levels of H_2O_2 inside autophagic vesicles increase upon starvation and also validated that **ROSA** was taken up in autophagic vesicles right at the early stages of autophagy.

The fluorescence lifetime data can be used to further confirm the extent of labeling for **ROSA**. When lifetime images were taken with a wider field of view, it was observed that all of the cells within the imaged plate were labeled with the sensor (Figure S16a). Therefore, the few cells, which appeared to be unlabeled in the fluorescence intensity images (Figure S11b), possibly also had incorporated the probe; but the fluorescence intensity was low due to the low extent of autophagy and concomitantly low levels of H_2O_2 within autophagic vesicles.

We next employed **ROSA** to assess the levels of H_2O_2 at different stages of autophagy. Since substantial levels of H_2O_2 have been reported to be present in lysosomes,[30,31,33] colocalization studies were performed with **ROSA** and **Lysotracker Red** in starved living cells (Figure S17). The punctate-like regions marked by **Lysotracker Red** also showed a significant fluorescence intensity from **ROSA**. However, some additional punctate regions with high intensity from **ROSA** were observed, which were not marked by **Lysotracker Red** (Mander's coefficients: M1 = 0.32, M2 = 0.86) (Figure S17). This proved that significant levels of H_2O_2 were present not only in lysosomes but also in other stages of autophagic vesicles.

We then asked the following question: At which stage of autophagy were the levels of H_2O_2 the highest within the compartments (Figure 5)? For identifying the autophagic phases of the vesicles, we utilized our previously reported ratiometric probe, **HCFP**,[7] that was capable of distinguishing the different stages of autophagy within autophagic vesicles: autophagosomes, autolysosomes, and lysosomes. Autophagic vesicles exhibit a pH transition from approximately 6−6.5 to 4.5 as they progress through different stages. Autophagosomes initially have a pH around 6−6.5. These vesicles encapsulate cellular waste for degradation. Autolysosomes form when autophagosomes fuse with lysosomes, resulting in a pH range of 5−5.5. The final stage of autophagic vesicles is lysosomes with a pH of 4.5. The acidic environment aids in the enzymatic breakdown of the contents. **HCFP** employs two dyes: fluorescein and hemicyanine.[7] During the progression of autophagy, the fluorescence of fluorescein decreases owing to the decrease in pH inside the autophagic vesicles and that of hemicyanine increases.[7] We generated a calibration plot based on the variation of the ratio of integrated fluorescence intensities in green and red channels obtained from the in vitro fluorescence titration of **HCFP** with pH (Figure 5b). Based on the calibration plot, we could correlate the ratio of green and red channel intensities with the reported pH inside different stages of autophagic vesicles and determine the specific ratios of green and red fluorescence associated with distinctive phases of autophagy (Figure 5b). Since one of the emission channels of **HCFP** (green) and that of **ROSA** have a significant overlap, we used excitation ratiometry for this experiment (Figure 5). Further, to confirm that there was no bleed-through between the **HCFP** green channel and **ROSA**, cells were only incubated with **ROSA** and imaged at the excitation wavelength and emission channel of **HCFP** and vice versa (Figure S18). In both cases, negligible fluorescence was observed. Cells in the resting state as well as after starvation were then incubated with both **HCFP** and **ROSA**. The fluorescence ratios obtained from different intracellular autophagic vesicles were analyzed to accurately distinguish

https://doi.org/10.1021/jacsau.4c01021
JACS Au 2025, 5, 343−352

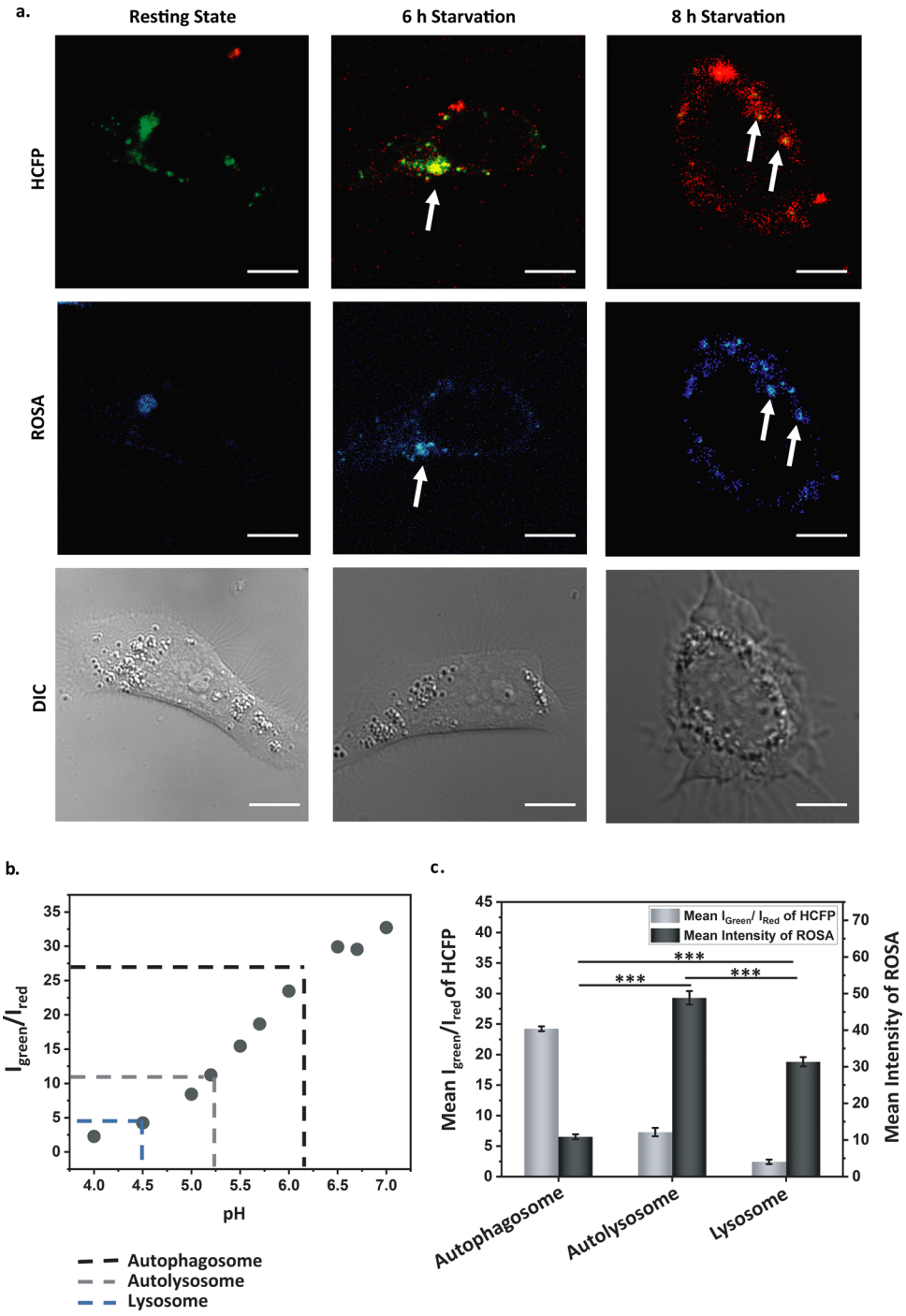

Figure 5. Representative confocal single z plane images of HeLa cells (first panel: overlay images of green and red channels, for **HCFP**, corresponding to λ_{ex} = 488 and 543 nm, λ_{em} = 500−561 nm (green), 575−650 nm (red); second panel: images corresponding to λ_{ex} = 405 nm, λ_{em} = 500−545 nm for **ROSA**; third panel: differential contrast images). Different sets of HeLa cells were starved for 0 (resting state), 6, and 8 h, respectively, then incubated with **ROSA** (10 μM) in aqueous media for 30 min, washed and incubated with **HCFP** (10 μM) in aqueous media for 30 min, and washed and imaged. White arrows mark the autolysosomes. (b) Variation of the ratio of the observed integrated fluorescence intensity in the green channel (I_{green}) (500−561 nm) and the red channel (I_{red}) (575−650 nm) over a pH range of 4−7. Ratios corresponding to the reported pH values of autophagosomes (black), autolysosomes (gray), and lysosomes (blue) have been marked via dotted lines. (c) Bar plots representing mean intensities obtained from intensity analysis of three sets of cells mentioned in panel (a). Data are presented as SEM, where n = 6 in each set.

and characterize various stages of autophagy in living cells. As shown in Figure 5a (top panel), the overlay of green and red channels reveals distinct phases of autophagy. Based on the ratios of green and red channels obtained, green regions depict autophagosomes, yellow regions represent autolysosomes, and lysosomes are represented by red regions. We then analyzed the relative fluorescence intensities of **ROSA** in the same intracellular autophagic vesicles (Figure 5a, midpanel). A very low intensity was observed in autophagosomes (Figure 5a, midpanel and c), indicating low H_2O_2 levels in the initial stage

https://doi.org/10.1021/jacsau.4c01021
JACS Au 2025, 5, 343−352

of autophagy. The intensity of **ROSA** increased significantly in lysosomes (Figure 5a, midpanel and c), which correlates with previous reports that indicate the presence of high H_2O_2 levels in lysosomes.[30,31,33] Interestingly, the maximum intensity of **ROSA** was recorded in autolysosomes (Figure 5a, midpanel and c).

We performed an identical experiment by triggering autophagy with Rapamycin treatment instead of starvation. Cells at the resting state, as well as after Rapamycin treatment, were incubated with both **HCFP** and **ROSA**. In this case as well, a very low intensity from the **ROSA** channel was observed in autophagosomes, a significantly enhanced intensity was observed in lysosomes, and maximum intensity was recorded in the autolysosomal stage (Figure S19).

Therefore, we could conclude that upon triggering autophagy, initially the levels of H_2O_2 are low, which increases to a maximum when the autophagosome fuses with the lysosome. The H_2O_2 levels decrease significantly in lysosomes compared to autolysosomes. However, the levels in lysosomes remain still significantly higher than those in autophagosomes. To the best of our knowledge, this is the first observation of fluctuations in H_2O_2 concentrations within autophagic compartments during the progression of different stages of autophagy in living mammalian cells.

CONCLUSIONS

This study offers new insights into the dynamic fluctuations of H_2O_2 across various stages of autophagic vesicles in living mammalian cells. By employing the novel sensors **ROSA** and **pHA**, we were able to simultaneously monitor H_2O_2 and pH inside autophagic vesicles during autophagy under different triggers. We further utilized the previously reported autophagy-targeted **HCFP** sensor to categorize the stages of autophagy and investigated the H_2O_2 levels in those identified stages of autophagic vesicles. Our findings revealed that H_2O_2 levels peaked during the autolysosome phase, shedding light on the oxidative fluctuations that occur as autophagy progresses. This work provides a comprehensive observation of the interplay between oxidative stress and autophagy. The probes developed in this study can aid in elucidating the mechanisms through which oxidative stress within autophagic compartments impacts cellular homeostasis and disease progression. Monitoring H_2O_2 levels in autophagic vesicles can serve as a biomarker for autophagy-related disorders, potentially helping in the early detection and assessment of conditions such as neurodegeneration, cardiovascular disorders, and cancer. Moreover, modulating H_2O_2 levels in autophagic vesicles may offer novel strategies for regulating autophagy, leading to more effective therapeutic approaches. Overall, our novel modular sensors, **ROSA** and **pHA**, and observations using these probes highlight the significance of oxidative regulation within autophagic compartments.

METHODS

Synthesis and Characterization of Molecules

Details of synthetic procedures are available in the Supporting Information. Novel molecules were characterized via liquid chromatography (LC) and low-resolution mass spectrometry (LRMS). Data are provided in the Supporting Information.

In Vitro Fluorescence Measurements

All spectroscopic measurements were performed at room temperature. Since both **ROSA** and **pHA** were completely water-soluble, all stock solutions were prepared in aqueous media. Solutions of **ROSA** (10 μM) and **pHA** (10 μM) were prepared from a primary stock in water by further dissolving in an aqueous buffer consisting of HEPES (20 mM) with the pH adjusted to 7.4. Fluorescence spectra were recorded on a FluoroLog-3 (Horiba Jobin Yvon Inc.) spectrofluorometer using quartz cuvettes with 10 mm × 2 mm inner dimensions (Hellma Analytics). Fluorescence spectra of **ROSA** were obtained by excitation at 378 nm with a slit width 5 nm for both excitation and emission, and those of **pHA** were obtained by excitation at 540 nm with a slit width 5 nm for both excitation and emission. H_2O_2 was used from a stock of 30% H_2O_2. The fluorescence response of **ROSA** was checked in the presence of 0 to 560 μM H_2O_2. The pH-dependent response of only **ROSA** and **ROSA** in the presence of H_2O_2 (560 μM) was also checked in the aqueous buffer (HEPES, 20 mM) of pH 4.5. Other biologically relevant analytes (Cl^-, NO_3^-, HCO_3^-, glutathione (GSH), and ascorbic acid) were used to test the selectivity of **ROSA** toward H_2O_2. Sodium (Na) salts of Cl^- and HCO_3^- and the potassium (K) salt of NO_3^- ions were used. To obtain the pH-dependent response for **pHA**, aqueous buffers (HEPES, 20 mM) of pH values 4, 5, 6, 7, and 8 were prepared either by adding few drops of HCl or NaOH. The pH-dependent fluorescence response of **pHA** was also checked in the presence of H_2O_2 (560 μM). The fluorescence of **pHA** was checked in the presence of physiologically relevant concentrations of essential metal ions (Na^+ (5 mM), K^+ (140 mM), Mg^{2+} (1 mM), Ca^{2+} (100 nM), Mn^{2+} (1 μM), Fe^{2+} (1 μM)), and GSH (500 μM) in the aqueous buffer of pH 7. Metal salts were used in the form of their chlorides for the experiment.

Cell Culture and Confocal Fluorescence Imaging

HeLa cells were cultured in DMEM (Sigma-Aldrich), supplemented with fetal bovine serum (10%, Gibco) and an antibiotic (100×, 10 mL/L) in T25 culture plates at 37 °C under humidified air containing 5% CO_2. For HeLa cells, additional glucose (3.5 mg/L) was added to the media. A day before the imaging, the cells were plated on homemade glass coverslip-bottomed Petri plates (35 mm diameter, Tarsons) coated with polylysine (200 μg/mL). Fluorescence images of the cells were recorded on a confocal microscope (LSM 880, Carl Zeiss, Germany) using 40× oil immersion objectives. A 405 nm laser was used as the excitation source for **ROSA** and emission was collected from 500 to 545 nm. A 543 nm laser was used as the excitation source for **pHA** and emission was collected from 575 to 650 nm. DMEM media without phenol red (pH adjusted to 7.4 or 4.5) was used during the confocal studies. Healthy HeLa cells were incubated with **ROSA** (10 μM) in DMEM media without phenol red at pH 7.4 for 30 min at 37 °C under humidified air containing 5% CO_2 and then washed and incubated with **pHA** (10 μM) for 30 min at 37 °C under humidified air containing 5% CO_2 to get the data corresponding to the resting state of cells. After staining, the cells were washed with the DMEM media without phenol red at pH 7.4 and imaged.

For inducing starvation, DMEM media from cells plated on homemade glass coverslip-bottomed Petri plates (35 mm diameter, Tarsons) coated with polylysine were removed and the cells were incubated with Hank's balanced salt solution (HBSS) for 6, 8, and 16 h, respectively. Following this, the cells were washed with DMEM media without phenol red at pH 7.4 and incubated with **ROSA** (10 μM) for 30 min, washed and incubated with **pHA** (10 μM) for 30 min, washed and imaged.

In order to trigger Rapamycin-induced autophagy, cells plated on homemade glass coverslip-bottomed Petri plates (35 mm diameter, Tarsons) coated with polylysine were incubated with Rapamycin (100 μM) in DMEM media without phenol red at pH 7.4 for 2, 4, 6, and 8 h, respectively. Following this, the cells were washed with DMEM media without phenol red at pH 7.4 and incubated with **ROSA** (10 μM) for 30 min, washed and incubated with **pHA** (10 μM) for 30 min, and washed and imaged.

For studying the autophagic vesicle targetability of the probes, CFP-LC3/GFP-LC3 plasmids were transiently transfected into a suspension of HeLa cells, using Lipofectamine 3000 in OptiMEM.

https://doi.org/10.1021/jacsau.4c01021
JACS Au 2025, 5, 343−352

The suspension was then plated on homemade glass coverslip-bottomed Petri plates (35 mm diameter, Tarsons) coated with polylysine (200 μg/mL). After 16 h of transfection, the cells were starved in HBSS buffer for 8 h. Following that, starved cells transfected with CFP-LC3 were incubated with **ROSA** (10 μM) for 30 min, washed, and imaged and starved cells transfected with GFP-LC3 were incubated with **pHA** (10 μM) for 30 min, washed, and imaged. A 405 nm laser was used as the excitation source for CFP-LC3 and emission was collected from 420 to 480 nm. A 488 nm laser was used as the excitation source for GFP-LC3 and emission was collected from 500 to 550 nm.

For testing the lysosomal localization of **ROSA**, HeLa cells were starved in HBSS buffer for 8 h. Following that, starved cells were incubated with **ROSA** (10 μM) for 30 min, washed and incubated with **Lysotracker Red** (100 nM) for 30 min, and washed and imaged. A 543 nm laser was used as an excitation source for **Lysotracker Red** and emission was collected from 575 to 650 nm.

In order to get information on H_2O_2 levels in different stages of autophagy, HeLa cells were starved in the HBSS buffer for 0, 6, and 8 h, respectively, or incubated with Rapamycin (100 nM) for 0 and 8 h, respectively. Following that, starved/Rapamycin-treated cells were incubated with **ROSA** (10 μM) for 30 min, washed and incubated with **HCFP** (10 μM) for 30 min, and washed and imaged. 488 and 543 nm lasers were used as excitation sources for **HCFP** and emission was collected in two channels, one from 500 to 561 nm (green channel) and the other from 570 to 650 nm (red channel). Since one of the emission channels of **HCFP** (green channel) and that of **ROSA** overlapped, excitation ratiometry was employed for this experiment.

■ ASSOCIATED CONTENT

Supporting Information

The Supporting Information is available free of charge at https://pubs.acs.org/doi/10.1021/jacsau.4c01021.

Experimental details of synthesis; LC-ESI-MS; in vitro fluorescence experiments; cell studies; fluorescence lifetime imaging, and image analysis (PDF)

■ AUTHOR INFORMATION

Corresponding Author

Ankona Datta − *Department of Chemical Sciences, Tata Institute of Fundamental Research, Mumbai 400005, India;* orcid.org/0000-0003-0821-6044; Email: ankona@tifr.res.in

Authors

Smitaroopa Kahali − *Department of Chemical Sciences, Tata Institute of Fundamental Research, Mumbai 400005, India;* orcid.org/0009-0004-5074-569X

Ranojoy Baisya − *Department of Chemical Sciences, Tata Institute of Fundamental Research, Mumbai 400005, India;* Present Address: Department of Chemistry, Indiana University, Bloomington 47405, United States

Sayani Das − *Department of Chemical Sciences, Tata Institute of Fundamental Research, Mumbai 400005, India;* Present Address: Merck & Co., Inc., Rahway, New Jersey, United States

Complete contact information is available at: https://pubs.acs.org/10.1021/jacsau.4c01021

Author Contributions

A.D. and S.K. designed and conceptualized the project, performed the experiments, analyzed the data, and wrote the paper. R.B. participated in the synthesis of the H_2O_2-sensitive dye and that of **pHA**. S.D. synthesized **HCFP**. All authors checked the results and the manuscript and approved the final version of the manuscript.

Notes

The authors declare no competing financial interest.

■ ACKNOWLEDGMENTS

A.D. acknowledges the support of the Department of Atomic Energy, Government of India under Project Identification No. RTI4003. The authors acknowledge Boby K.V. for the help with FLIM experiments; Sandhya Koushika and Sneha Hegde for CFP-LC3 and GFP-LC3; Mahendra Sonawane and Shravani R.S. for providing Rapamycin; and the DCS Cell Culture facility, TIFR, Mumbai.

■ REFERENCES

(1) Yamamoto, H.; Zhang, S.; Mizushima, N. Autophagy genes in biology and disease. *Nat. Rev. Genet.* **2023**, *24* (6), 382−400.

(2) Doherty, J.; Baehrecke, E. H. Life, death and autophagy. *Nat. Cell Biol.* **2018**, *20* (10), 1110−1117.

(3) Levine, B.; Kroemer, G. Autophagy in the Pathogenesis of Disease. *Cell* **2008**, *132* (1), 27−42.

(4) Khandia, R.; Dadar, M.; Munjal, A.; Dhama, K.; Karthik, K.; Tiwari, R.; Yatoo, M. I.; Iqbal, H. M. N.; Singh, K. P.; Joshi, S. K.; Chaicumpa, W. A Comprehensive Review of Autophagy and Its Various Roles in Infectious, Non-Infectious, and Lifestyle Diseases: Current Knowledge and Prospects for Disease Prevention, Novel Drug Design, and Therapy. *Cells* **2019**, *8* (7), 674.

(5) Ichimiya, T.; Yamakawa, T.; Hirano, T.; Yokoyama, Y.; Hayashi, Y.; Hirayama, D.; Wagatsuma, K.; Itoi, T.; Nakase, H. Autophagy and Autophagy-Related Diseases: A Review. *Int. J. Mol. Sci.* **2020**, *21* (23), 8974.

(6) Maulucci, G.; Chiarpotto, M.; Papi, M.; Samengo, D.; Pani, G.; De Spirito, M. Quantitative analysis of autophagic flux by confocal pH-imaging of autophagic intermediates. *Autophagy* **2015**, *11* (10), 1905−1916.

(7) Das, S.; Kapadia, A.; Pal, S.; Datta, A. Spatio-Temporal Autophagy Tracking with a Cell-Permeable, Water-Soluble, Peptide-Based, Autophagic Vesicle-Targeted Sensor. *ACS Sens.* **2021**, *6* (6), 2252−2260.

(8) Chen, Y.; McMillan-Ward, E.; Kong, J.; Israels, S. J.; Gibson, S. B. Oxidative stress induces autophagic cell death independent of apoptosis in transformed and cancer cells. *Cell Death Differ.* **2008**, *15* (1), 171−182.

(9) Chen, Y.; Azad, M. B.; Gibson, S. B. Superoxide is the major reactive oxygen species regulating autophagy. *Cell Death Differ.* **2009**, *16* (7), 1040−1052.

(10) Filomeni, G.; De Zio, D.; Cecconi, F. Oxidative stress and autophagy: the clash between damage and metabolic needs. *Cell Death Differ.* **2015**, *22* (3), 377−388.

(11) Yun, H. R.; Jo, Y. H.; Kim, J.; Shin, Y.; Kim, S. S.; Choi, T. G. Roles of Autophagy in Oxidative Stress. *Int. J. Mol. Sci.* **2020**, *21* (9), 3289.

(12) Song, S. B.; Hwang, E. S. High Levels of ROS Impair Lysosomal Acidity and Autophagy Flux in Glucose-Deprived Fibroblasts by Activating ATM and Erk Pathways. *Biomolecules* **2020**, *10* (5), 761.

(13) Scherz-Shouval, R.; Shvets, E.; Fass, E.; Shorer, H.; Gil, L.; Elazar, Z. Reactive oxygen species are essential for autophagy and specifically regulate the activity of Atg4. *EMBO J.* **2007**, *26* (7), 1749−1760−1760.

(14) Kubota, C.; Torii, S.; Hou, N.; Saito, N.; Yoshimoto, Y.; Imai, H.; Takeuchi, T. Constitutive Reactive Oxygen Species Generation from Autophagosome/Lysosome in Neuronal Oxidative Toxicity*. *J. Biol. Chem.* **2010**, *285* (1), 667−674.

(15) Sango, J.; Kakihana, T.; Takahashi, M.; Katsuragi, Y.; Anisimov, S.; Komatsu, M.; Fujii, M. USP10 inhibits the dopamine-induced reactive oxygen species−dependent apoptosis of neuronal cells by

stimulating the antioxidant Nrf2 activity. *J. Biol. Chem.* **2022**, *298* (1), No. 101448.
(16) Talebi, M.; Mohammadi Vadoud, S. A.; Haratian, A.; Talebi, M.; Farkhondeh, T.; Pourbagher-Shahri, A. M.; Samarghandian, S. The interplay between oxidative stress and autophagy: focus on the development of neurological diseases. *Behav. Brain Funct.* **2022**, *18* (1), 3.
(17) Bhatia, V.; Sharma, S. Role of mitochondrial dysfunction, oxidative stress and autophagy in progression of Alzheimer's disease. *J. Neurol. Sci.* **2021**, *421*, No. 117253.
(18) Xiao, B.; Kuruvilla, J.; Tan, E.-K. Mitophagy and reactive oxygen species interplay in Parkinson's disease. *npj Parkinson's Dis.* **2022**, *8* (1), 135.
(19) Poillet-Perez, L.; Despouy, G.; Delage-Mourroux, R.; Boyer-Guittaut, M. Interplay between ROS and autophagy in cancer cells, from tumor initiation to cancer therapy. *Redox Biol.* **2015**, *4*, 184−192.
(20) Peng, Y.; Tao, Y.; Liu, L.; Zhang, J.; Wei, B. Crosstalk among Reactive Oxygen Species, Autophagy and Metabolism in Myocardial Ischemia and Reperfusion Stages. *Aging Dis.* **2024**, *15* (3), 1075−1107.
(21) Ma, X.; Liu, H.; Foyil, S. R.; Godar, R. J.; Weinheimer, C. J.; Diwan, A. Autophagy is impaired in cardiac ischemia-reperfusion injury. *Autophagy* **2012**, *8* (9), 1394−1396.
(22) Sciarretta, S.; Hariharan, N.; Monden, Y.; Zablocki, D.; Sadoshima, J. Is Autophagy in Response to Ischemia and Reperfusion Protective or Detrimental for the Heart? *Pediatr. Cardiol.* **2011**, *32* (3), 275−281.
(23) Gonzalez, C. D.; Lee, M.-S.; Marchetti, P.; Pietropaolo, M.; Towns, R.; Vaccaro, M. I.; Watada, H.; Wiley, J. W. The emerging role of autophagy in the pathophysiology of diabetes mellitus. *Autophagy* **2011**, *7* (1), 2−11.
(24) Yuan, Y.; Chen, Y.; Peng, T.; Li, L.; Zhu, W.; Liu, F.; Liu, S.; An, X.; Luo, R.; Cheng, J.; Liu, J.; Lu, Y. Mitochondrial ROS-induced lysosomal dysfunction impairs autophagic flux and contributes to M1 macrophage polarization in a diabetic condition. *Clin. Sci.* **2019**, *133* (15), 1759−1777.
(25) Perillo, B.; Di Donato, M.; Pezone, A.; Di Zazzo, E.; Giovannelli, P.; Galasso, G.; Castoria, G.; Migliaccio, A. ROS in cancer therapy: the bright side of the moon. *Exp. Mol. Med.* **2020**, *52* (2), 192−203.
(26) Sedlackova, L.; Korolchuk, V. I. The crosstalk of NAD, ROS and autophagy in cellular health and ageing. *Biogerontology* **2020**, *21* (3), 381−397.
(27) Pietrocola, F.; Bravo-San Pedro, J. M. Targeting Autophagy to Counteract Obesity-Associated Oxidative Stress. *Antioxidants* **2021**, *10* (1), 102.
(28) Dong, L.; He, J.; Luo, L.; Wang, K. Targeting the Interplay of Autophagy and ROS for Cancer Therapy: An Updated Overview on Phytochemicals. *Pharmaceuticals* **2023**, *16*, 92.
(29) Zhou, R.; Peng, Q.; Wan, D.; Yu, C.; Zhang, Y.; Hou, Y.; Luo, Q.; Li, X.; Zhang, S.; Xie, L.; Ou, P.; Peng, Y. Construction of a lysosome-targetable ratiometric fluorescent probe for H_2O_2 tracing and imaging in living cells and an inflamed model. *RSC Adv.* **2021**, *11* (39), 24032−24037.
(30) Saffi, G. T.; Tang, E.; Mamand, S.; Inpanathan, S.; Fountain, A.; Salmena, L.; Botelho, R. J. Reactive oxygen species prevent lysosome coalescence during PIKfyve inhibition. *PLoS One* **2021**, *16* (11), No. e0259313.
(31) Zhang, X.; Cheng, X.; Yu, L.; Yang, J.; Calvo, R.; Patnaik, S.; Hu, X.; Gao, Q.; Yang, M.; Lawas, M.; Delling, M.; Marugan, J.; Ferrer, M.; Xu, H. MCOLN1 is a ROS sensor in lysosomes that regulates autophagy. *Nat. Commun.* **2016**, *7* (1), No. 12109.
(32) Nguyen, V.-N.; Li, H. Recent Development of Lysosome-Targeted Organic Fluorescent Probes for Reactive Oxygen Species. *Molecules* **2023**, *28* (18), 6650.
(33) Feng, B.; Ma, Y.; Zheng, F.; Huang, X.; Feng, X.; Zhang, K.; Liu, L.; Chen, F.; Zeng, W. Development of near-infrared lysosomal pH-activatable fluorescent probe for real-time visualization of autophagy progression. *Chem. Eng. J.* **2023**, *464*, No. 142554.
(34) Hou, L.; Ning, P.; Feng, Y.; Ding, Y.; Bai, L.; Li, L.; Yu, H.; Meng, X. Two-Photon Fluorescent Probe for Monitoring Autophagy via Fluorescence Lifetime Imaging. *Anal. Chem.* **2018**, *90* (12), 7122−7126.
(35) Kim, D.; Kim, G.; Nam, S.-J.; Yin, J.; Yoon, J. Visualization of Endogenous and Exogenous Hydrogen Peroxide Using A Lysosome-Targetable Fluorescent Probe. *Sci. Rep.* **2015**, *5* (1), No. 8488.
(36) Huang, X.; Chen, F.; Ma, Y.; Zheng, F.; Fang, Y.; Feng, B.; Huang, S.; Zeng, H.; Zeng, W. De novo design of a novel AIE fluorescent probe tailored to autophagy visualization via pH manipulation. *Biomater. Res.* **2023**, *27* (1), 20.
(37) Xu, F.; Li, H.; Yao, Q.; Fan, J.; Wang, J.; Peng, X. A NIR fluorescent probe: imaging endogenous hydrogen peroxide during an autophagy process induced by rapamycin. *J. Mater. Chem. B* **2016**, *4* (46), 7363−7367.
(38) Yu, L.; Chen, Y.; Tooze, S. A. Autophagy pathway: Cellular and molecular mechanisms. *Autophagy* **2018**, *14* (2), 207−215.
(39) Noda, N. N.; Ohsumi, Y.; Inagaki, F. Atg8-family interacting motif crucial for selective autophagy. *FEBS Lett.* **2010**, *584* (7), 1379−1385.
(40) Noda, N. N.; Kumeta, H.; Nakatogawa, H.; Satoo, K.; Adachi, W.; Ishii, J.; Fujioka, Y.; Ohsumi, Y.; Inagaki, F. Structural basis of target recognition by Atg8/LC3 during selective autophagy. *Genes Cells* **2008**, *13* (12), 1211−1218.
(41) Ichimura, Y.; Kumanomidou, T.; Sou, Y.-s.; Mizushima, T.; Ezaki, J.; Ueno, T.; Kominami, E.; Yamane, T.; Tanaka, K.; Komatsu, M. Structural Basis for Sorting Mechanism of p62 in Selective Autophagy*. *J. Biol. Chem.* **2008**, *283* (33), 22847−22857.
(42) Fuchs, S. M.; Raines, R. T. Pathway for Polyarginine Entry into Mammalian Cells. *Biochemistry* **2004**, *43* (9), 2438−2444.
(43) Ren, M.; Deng, B.; Wang, J.-Y.; Kong, X.; Liu, Z.-R.; Zhou, K.; He, L.; Lin, W. A fast responsive two-photon fluorescent probe for imaging H_2O_2 in lysosomes with a large turn-on fluorescence signal. *Biosens. Bioelectron.* **2016**, *79*, 237−243.
(44) Liang, X.; Zhang, L.; Xu, X.; Qiao, D.; Shen, T.; Yin, Z.; Shang, L. An ICT-Based Mitochondria-Targeted Fluorescent Probe for Hydrogen Peroxide with a Large Turn-On Fluorescence Signal. *ChemistrySelect* **2019**, *4* (4), 1330−1336.
(45) Shen, Y.; Zhang, X.; Huang, X.; Zhang, Y.; Zhang, C.; Jin, J.; Liu, X.; Li, H.; Yao, S. A new fluorescence and colorimetric sensor for highly selective and sensitive detection of glucose in 100% water. *RSC Adv.* **2015**, *5* (78), 63226−63232.
(46) Dong, H.-Q.; Wei, T.-B.; Ma, X.-Q.; Yang, Q.-Y.; Zhang, Y.-F.; Sun, Y.-J.; Shi, B.-B.; Yao, H.; Zhang, Y.-M.; Lin, Q. 1,8-Naphthalimide-based fluorescent chemosensors: recent advances and perspectives. *J. Mater. Chem. C* **2020**, *8* (39), 13501−13529.
(47) Swanson, W. B.; Durdan, M.; Eberle, M.; Woodbury, S.; Mauser, A.; Gregory, J.; Zhang, B.; Niemann, D.; Herremans, J.; Ma, P. X.; Lahann, J.; Weivoda, M.; Mishina, Y.; Greineder, C. F. A library of Rhodamine6G-based pH-sensitive fluorescent probes with versatile in vivo and in vitro applications. *RSC Chem. Biol.* **2022**, *3* (6), 748−764.
(48) White, E.; Lattime, E. C.; Guo, J. Y. Autophagy Regulates Stress Responses, Metabolism, and Anticancer Immunity. *Trends Cancer* **2021**, *7* (8), 778−789.
(49) Kristensen, A. R.; Schandorff, S.; Høyer-Hansen, M.; Nielsen, M. O.; Jaüaüttelaü, M.; Dengjel, J.; Andersen, J. S. Ordered Organelle Degradation during Starvation-induced Autophagy. *Mol. Cell. Proteomics* **2008**, *7* (12), 2419−2428.
(50) Shang, L.; Chen, S.; Du, F.; Li, S.; Zhao, L.; Wang, X. Nutrient starvation elicits an acute autophagic response mediated by Ulk1 dephosphorylation and its subsequent dissociation from AMPK. *Proc. Natl. Acad. Sci. U.S.A.* **2011**, *108* (12), 4788−4793.
(51) Wen, Y.; Liu, K.; Yang, H.; Li, Y.; Lan, H.; Liu, Y.; Zhang, X.; Yi, T. A Highly Sensitive Ratiometric Fluorescent Probe for the Detection of Cytoplasmic and Nuclear Hydrogen Peroxide. *Anal. Chem.* **2014**, *86* (19), 9970−9976.

https://doi.org/10.1021/jacsau.4c01021
JACS Au 2025, 5, 343−352